RSC Advances

ROYAL SOCIETY OF CHEMISTRY

www.rsc.org/advances

Graphical abstract (TOC)

Correlation between Surface Chemistry, Gasochromism and Field emission Properties of Tungsten Oxide Nanowire Thin Films When Exposure to Atomic Oxygen

C. X. Zhao,[a,b] S. Z. Deng,[a] N. S. Xu[a] and Jun Chen,[a†]

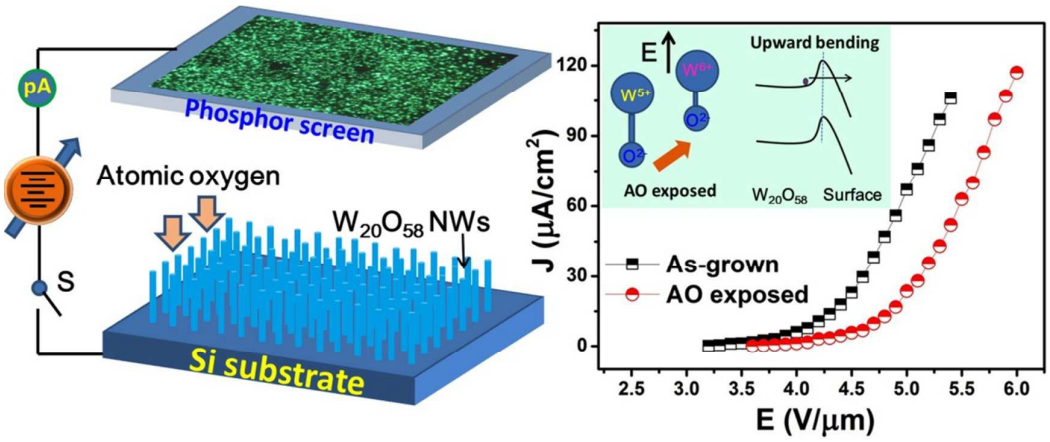

The effects of atomic oxygen (AO) exposure on the surface chemistry, gasochromism, field emission properties of vetically aligned $W_{20}O_{58}$ nanowires have been investigated. Work function measurement indicates that Fermi level has a distinctive decrease of ~0.29 eV after AO exposure. The W valence state shows a clear transition from +5 to +6, corresponding to AO exposure induced color bleaching process. The origin of work function raise is ascribed to the strengthened surface dipole, which is the main reason that accounts for the observed field emission characteristics.

RSC Advances

ARTICLE

Correlation between Surface Chemistry, Gasochromism and Field emission Properties of Tungsten Oxide Nanowire Thin Films When Exposure to Atomic Oxygen

Received 24th June 2015,
Accepted 00th January 2015

DOI: 10.1039/x0xx00000x

www.rsc.org/

C. X. Zhao,[a,b] S. Z. Deng,[a] N. S. Xu[a] and Jun Chen[a†]

Excellent field emission is observed from vetically aligned $W_{20}O_{58}$ nanowires that are prepared by thermal evaporation. The effects of atomic oxygen (AO) exposure on its surface chemistry, gasochromism, field emission properties have been investigated. Morphology and structural characterization indicates little change was observed in the nanowire after high dose of AO exposure. It's worth noting that stable and high emission current could be kept, with a little increase of turn-on electric field (defined at 10 μA/cm^2). Work function measurement indicates that Fermi level has a distinctive decrease of ~0.29 eV after AO exposure. The W valence state shows a clear transition from +5 to +6, corresponding to AO exposure induced color bleaching process. The origin of work function raise is ascribed to the strengthened surface dipole, which is the main reason that accounts for the observed field emission characteristics.

1. Introduction

Tungsten oxide has been extensively studied for its wide applications, such as information display, smart window, sensor devices, photo-catalyst, field emitters, synergetic therapy and so on.[1,2-4] Nanostructuring of tungsten oxide can enhance its performance and provides unique properties.[5] For example, tungsten oxide nanomaterials has exceptional fast gaschromic properties than its bulk forms.[2, 6] Sharp and aligned tungsten oxide nanowire arrays show excellent field emission performance.[7]

Due to the rich oxidation states of W element, tungsten oxide thin films are excellent oxidative gas sensor. Previous studies indicate that surface chemistry shows close relationship with transmittance, work function as well as conductivity.[6, 8] For instance, the coloration of tungsten oxide film when exposure to reducing H_2 is widely described by the transition of the W valence state from +6 to +5.[2] It was noted that the conductivity of WO_x would decrease proportionally to the amount of oxidative gas, while the reverse is for reducing gases.[9] Because the B/S(Body volume/Surface area) of nanowire is <10 nm in our study, the position of Fermi level is largely dependent on B/S.[10] Determine the position of Fermi level would be greatly demand for WO_x-based sensors which are selectively sensing to ozone gas.[10] Therefore, further investigation of the shift of Fermi level would provide in-depth evidence for understanding the selectivity of tungsten oxide gas sensor.

Since field emission process is highly dependent on the surface properties of cold cathode, it is of great significance to investigate the effect of different gas exposure on its field emission characteristic. It has been reported that tungsten oxide nanowire thin films possess excellent field emission property.[11] Previous study has confirmed that the emission uniformity of tungsten oxide field emitters could be largely improved by in situ hydrogen exposure.[12] However, the effect of oxidative gas exposure on the field emission property of tungsten oxides is still less studied[13] and needs further investigation.

In the present work, atomic oxygen exposure was adopted to study the effect surface state on the field emission property of $W_{20}O_{58}$ nanowires. We focus on the correlation between surface chemistry, gasochromic and field emission characteristics of $W_{20}O_{58}$ nanowire thin films. Finally, based on the experimental and calculated results, the corresponding mechanism is proposed.

2. Experimental

Large scale, high-dense, vertically aligned of $W_{20}O_{58}$ nanowires were grown on n-type silicon substrate by a high temperature, catalyst-free, thermal evaporation method.[7] The morphology and structure were characterized by scanning electron microscopy (SEM) and transmission electron microscopy (TEM). The atomic

[a] State Key Laboratory of Optoelectronic Materials and Technologies, Guangdong Province Key Laboratory of Display Material and Technology, and School of Physics and Engineering, Sun Yat-sen University, Guangzhou 510275, People's Republic of China
[b] Department of Physics and Siyuan Laboratory, Jinan University, Guangzhou, Guangzhou 510632, People's Republic of China
† Correspondence: stscjun@mail.sysu.edu.cn.
Tel: +86(20)-84113296 Fax: +86(20)84037855

oxygen exposure was conducted in an ultraviolet ozone cleaning system (Model 576-220 UV-Ozone cleaner, Jelight Co., Inc.). The ozone with concentration more than 1000 ppm was monitored and the atomic oxygen (AO) flux was estimated to be the order of $10^{23}/m^2s$ by assuming temperature in ozone source was 300 K,[8] the treating time is set to be 30 min. Chemical composition and work function were measured by X-ray photoelectric spectroscopy (XPS: ESCALAB 250 system, Al Kα X-rays 1486.6 eV, calibrate by C1s 248.8 eV) before and after AO exposure. During the work function measurement, a -5 V bias was applied to the samples during the measurements in order to distinguish the analyzer and the sample secondary electron emission cut-offs. Field emission measurement of $W_{20}O_{58}$ nanowires was carried out in an ultra-high vacuum chamber with base pressure ~5.0×10^{-7} Pa using a diode configuration.

3. Results and discussion

Fig. 1(a), (b) and (c) show typical SEM images of as-grown $W_{20}O_{58}$ nanowires with plane view, 45° inclination view and cross section view, respectively. The obtained $W_{20}O_{58}$ nanowires show dense distribution and with flat tip. The average length and tip radius of nanowire is 5.8 μm and 20±5 nm, respectively. Energy dispersive X-ray spectroscopy (EDS) analysis was conducted from the $W_{20}O_{58}$ nanowires and shown in Fig. 1(d). Besides the Si signals coming from the substrate, only W and O are detected. The chemical composition is consistent with $W_{20}O_{58}$ phase. The detailed microstructure of the $W_{20}O_{58}$ nanowire was further characterized by TEM. Fig.1(e,f) shows typical TEM image and HRTEM image of individual nanowire, respectively. The space fringe of ~0.38 nm is indexed to be the (010) plane of $W_{20}O_{58}$. The nanowires possess single crystalline nature with its axis direction in the [010] direction.

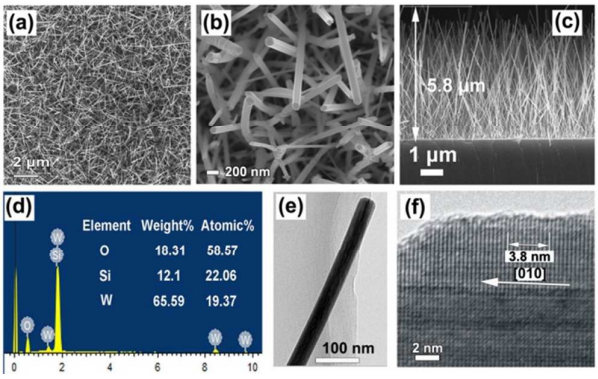

Fig. 1. SEM images of as-grown $W_{20}O_{58}$ nanowires, **(a)** plane view, **(b)** 45° inclination view, **(c)** cross section view, **(d)** EDS spectrum, and **(e, f)** TEM and HRTEM images, respectively.

Fig. 2(a,b) shows the typical X-ray diffraction pattern before and after ozone exposure, all the peaks are indexed to a monoclinic $W_{20}O_{58}$ phase (JCPDS#: 36-0101). The intensity of peaks (010) and (020) are much larger than its standard pattern, which implies a preferential growth along <010> direction. The result is consistent with the above HRTEM analysis. Inset of Fig. 2 gives the typical high resolution SEM images before and after ozone exposure. It indicates that ozone exposure has little effect on the morphology and structure of nanowire.

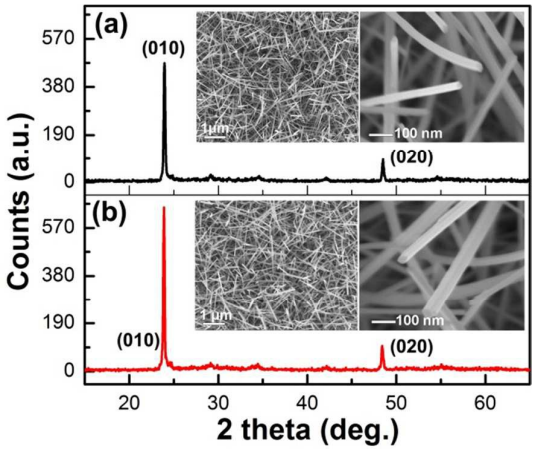

Fig.2. Typical X-ray diffraction patterns of as-grown nanowires (a) and ozone exposed nanowires (b).

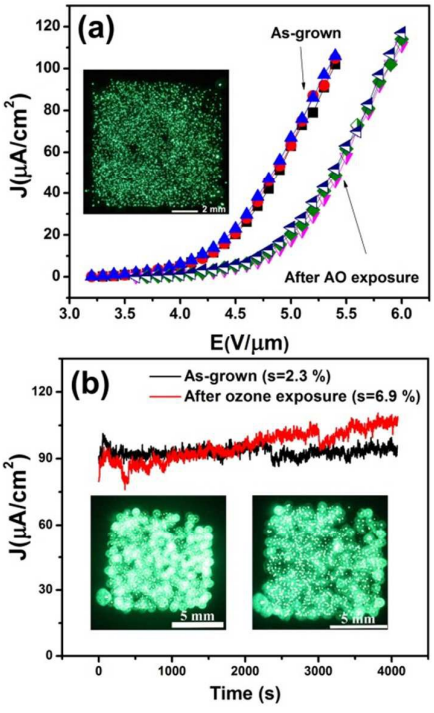

Fig. 3 (a) field emission current density versus electric field (J-E) curves of $W_{20}O_{58}$ nanowires before and after ozone exposure, inset shows the typical emission images. **3(b)** shows the corresponding emission current stability and emission images.

The typical field emission characteristics of $W_{20}O_{58}$ nanowires before and after ozone exposure are shown in Fig. 3. The turn-on field is defined as the electrical field to

obtain a current density of 10 μA/cm^2. It was found that the turn-on field increased from 4.2 V/μm to 4.8 V/μm after ozone exposure. The uniform emission sites are observed for the sample before ozone exposure, shown in Fig.3(a). The field emission current stability is measured under a constant voltage. In Fig. 3(b), the fluctuation is calculated to be 2.3 % and 6.9 % for the sample before and after ozone exposure, respectively. The corresponding emission images are shown in the inset of Fig. 3(b).

The obtained J-E curves were further analyzed on the basis of the classical Fowler-Nordheim (*FN*) theory. Fig. 4(a) shows the linear relationship of F-N plots derived from the above J-E curves, and the *FN* enhancement factor β could be estimated by the equation of β=-6830$\phi^{3/2}$/k.[8] where k is the slop of F-N plot and ϕ is the work function. Since the morphology of $W_{20}O_{58}$ nanowire show little change after high dose of atomic oxygen exposure, and the β value should keep constant (see Fig. 2(a, b)). Field emission performance of cathode depends exponentially on work function, as given by F-N theory. The decreased field emission current is probably ascribed to the change of work function.

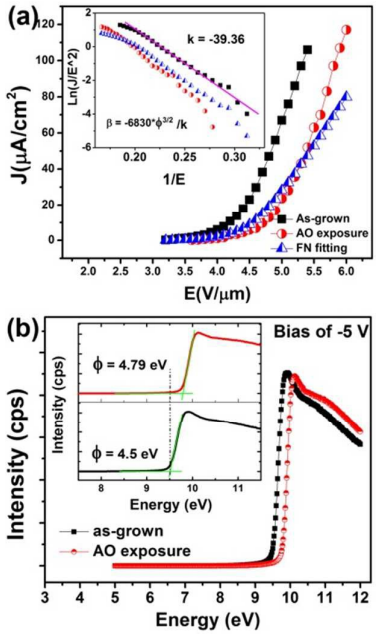

Fig. 4 (a) Experimental J-E curves and the calculated *J-E* curves, **(b)** work function measurements of $W_{20}O_{58}$ nanowire thin films before and after ozone exposure.

As shown in Fig. 4(b), work functions of the as-grown and AO exposed $W_{20}O_{58}$ nanowires were measured by low intensity X-ray photoelectron spectroscopy. The work function value was determined directly from the spectra by fitting straight lines into their low energy cut-off and determining the intersection with the base line of the spectra.[14,15] We found that it has a distinctive increase (~0.29 eV) after exposure. Work function values for as-grown and AO exposed $W_{20}O_{58}$ nanowires is 4.5 eV and ~4.79 eV, respectively.

Since the value of ϕ and β could be obtained, the field emission characteristic of $W_{20}O_{58}$ nanowire thin films could be deduced from the F-N theory by the following equation (1).

$$J_{AO}=\frac{J_0}{\phi_{AO}/\phi_0}\left\{\exp\frac{-B}{\beta E}(\phi_{AO}^{3/2}-\phi_0^{3/2})\right\} \quad (1)$$

Where J_0 is the field emission current density of $W_{20}O_{58}$ nanowires before AO exposure. B is a constant of 6.83×10^3 eV$^{-3/2}$.Vμm^{-1}, ϕ_0 and ϕ_{AO} is the work function of $W_{20}O_{58}$ nanowires before and after AO exposure, respectively. Fig. 4(a) gives the inverse calculated J-E curve with that of experimental curve. It indicates that the two curves are in reasonable agreement with each other. We believe that the decreased field emission current of AO exposed $W_{20}O_{58}$ nanowires is largely reason from the increase of surface work function.

Due to the nonstoichimetric of $W_{20}O_{58}$, oxygen vacancy inevitably exists on the surface of nanowires. Due to the larger electronegativity of O, the outer shell electrons can be transferred from W to O. High density of outer shell electrons surround O, which would induce the increase of core level binding energy of O_{1s} due to the enhanced screen effect. The screen effect was confirmed by detecting the core-level binding-energy shifts, which will be discussed in the following XPS analysis. Since more electrons concentrate on the surface, and dipole would be established with the orientation from inner nanowire to the vacuum. The origin of raised work function could be understood by the strengthened surface dipoles. Since the W valence state is increased from W^{5+} to W^{6+}, the energy band would be lifted due to the enhanced surface dipole (⊕→⊖). More discussion will be given in the following XPS analysis. Therefore, it is reasonable to understand the raised work function from the perspective of surface dipole. The higher the work function, the lower emission efficiency of electron from materials to vacuum.

The work function shows close relationship with surface chemical composition. In order to investigate the origin of work function change, surface chemistry states of W and O elements were also measured by high resolution XPS technique. Fig.5(a) shows the XPS spectrum of W_{4f}, it could be deconvoluted into five peaks. The binding energy peak locates at 34.05 eV, 35.8 eV, 36.2 eV, 37.95 eV, 40.89 eV corresponding to $W^{5+}4f_{7/2}$, $W^{6+}4f_{7/2}$, $W^{5+}4f_{5/2}$, $W^{6+}4f_{5/2}$, $W5p_{3/2}$, respectively.[16, 17] However, all the peaks of W_{4f} show a little blueshift to the higher energy side after AO exposure. The chemistry states of tungsten with or without ozone exposure were derived from the evolution of line shape of spectra. The ratio of W^{5+}/W^{6+} for $W_{20}O_{58}$ nanowires before and after AO exposure is determined to be 97.3 % and 55.6 %, respectively.

Fig. 5(b) shows the XPS spectrum of O_{1s}, the spectrum can be fitted into two components, the peaks

locate at 530.5 eV and 532.1 eV which corresponding to the binding energy of lattice oxygen in $W_{20}O_{58}$ (O-W) and chemisorbed oxygen (O-adsorption), respectively.[18] It was found that the two peaks show blueshift (~0.21 eV) to the higher energy side after AO exposure. The binding peaks of W_{4f} and O_{1s} shift in the same direction indicating the decrease of local electron density and downward-shift of Fermi level.[8] This agrees with the observed increase of work function from the perspective of band diagram analysis. The chemical state of O could be estimated by analyzing the integrated intensity area of divided peaks, namely, $S_{O\text{-}W}$ and $S_{O\text{-}adsorption}$. The relative ratio of $S_{O\text{-}W}$ to $S_{O\text{-}adsorption}$ shows a clear decrease from 96 % to 74.7 %, which indicates the amount of chemisorbed oxygen increased more than O-W after AO exposure.

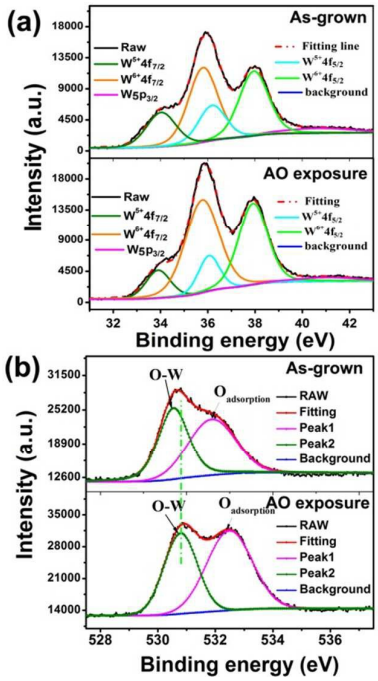

Fig. 5 (a,b) Curve fitting of the W_{4f} and O_{1s} binding energy peak in XPS spectrum of the $W_{20}O_{58}$ nanowire thin films, respectively.

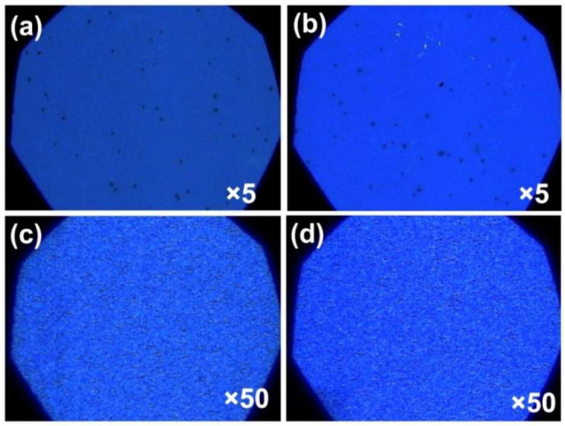

Fig. 6. Optical microscopy images of $W_{20}O_{58}$ nanowire thin films: **(a,c)** before and **(b,d)** after ozone exposure, respectively.

The gasochromism is usually observed when exposure to hydrogen gas, which is ascribed to the transition of W valence state from 6+ to 5+, and "generation of oxygen vacancies" model is usually proposed for such chromism.[19] However, the reverse case is in the AO exposure (oxidative gas) process. The W valence state would be increased from 5+ to 6+. The further oxidation of surface W valence would induce the bleaching of color. We propose that AO exposure would induce the "annihilation of oxygen vacancy". Therefore, it is likely to see the bleached state of $W_{20}O_{58}$ nanowire thin films after exposure to AO.

Fig. 6(a~d) give the typical optical images of the same sample obtained before and after AO exposure. Because the tungsten oxide was grown on silicon substrate, the image is obtained by the reflection color. Although the color contrast is not obvious, details could be found after careful observation. It shows that the surface color gradually changed from dark blue to light blue. This process is consistent with the beaching state for the reduced light adsorption. Namely, more light would be reflected for AO exposed $W_{20}O_{58}$ nanowire thin film. Therefore, brighter color image was observed. Due to the high crystalline nature of as-grown $W_{20}O_{58}$ nanowire, it shows a smaller degree of color change when compared to their amorphous counterpart.[20] Based on the aforementioned XPS analysis, the amount of lattice oxygen is increased after AO exposure. The density of surface oxygen vacancy would be decreased. Our experiment finding is in accordance with the bleaching state of tungsten oxide when exposure to oxygen.[21]

4. Conclusions

The effect of atomic oxygen (AO) exposure on the field emission properties of $W_{20}O_{58}$ nanowires has been investigated. It was found that the field emission turn-on electric field increased after AO exposure. Surface chemistry and work function of $W_{20}O_{58}$ before and after AO exposure have been obtained by XPS technique. AO exposure would induce further oxidation of surface, and the core level binding energy peaks of O_{1s} and W_{4f} shift in opposite direction. Meanwhile, surface work function was measured to be increased by ~0.29 eV. Based on the calculation, the raise of work function was mainly accounts for the increase of turn-on field. Finally, close relationship between surface chemistry, gasochromism and field emission have been found. The bleached color and lowered field emission current were considered to be originated from the transition of W valence state from +5 to 6+. It is worth noting that the stable and high field emission current makes $W_{20}O_{58}$ nanowire thin films a promising candidate for cold cathode in oxidative environment.

Acknowledgements

The authors gratefully acknowledge the financial support for the project from the National Key Basic Research Program of China (Grant Nos. 2010CB327703, 2007CB935501), the National Natural Science Foundation of China (Grant No. 60925001), the Fundamental Research Funds for the Central Universities (Grants Nos. 21615309), the Guangdong Natural Science Foundation (Grants Nos. 2014A030310302), the Science and Technology Department of Guangdong Province, the Economic and Information Industry Commission of Guangdong Province, and the Science & Technology and Information Department of Guangzhou City.

Notes and references

1 Y. B. Li, Y. Bando, and D. Golberg, Adv. Mater., 2003, **15**, 1294-1296.
2 H. Zheng, J. Z. Ou, M. S. Strano, R. B. Kaner, A. Mitchell, K. and Kalantar-zadeh, Adv. Fun. Mater., 2011, 21, 2175-2196.
3 P. Kalluru, R. Vankayala, C.-S. Chiang and K. C. Hwang, Angew. Chem. Int. Edit., 2013, **52**, 12332-12336.
4 B. J.-W. Liu, J. Zheng, J.-L. Wang, J. Xu, H.-H. Li and S.-H. Yu, Nano Lett. 2013, **13**, 3589-3593.
5 K. Kalantar-zadeh, B. Fry, *Nanotechnology-enabled sensors*. (Springer Science & Business Media, 2007).
6 S. Chen, J. Luo, H. Tan, J. Chen, S. Deng, and N. Xu, Sensors Actuat B-Chem., 2012, **173**, 824-832.
7 X. Zhang, L. Gong, K. Liu, Y. Cao, X. Xiao, W. Sun, X. Hu, Y. Gao, J. Chen and J. Zhou, Adv. Mater., 2010, **22**, 5292-5296.
8 C. X. Zhao, K. Huang, S. Z. Deng, N. S. Xu and J. Chen, Appl. Surf. Sci., 2013, **270**, 82-89.
9 X. L. Li, T. J. Lou, X. M. Sun and Y. D. Li, Inorg. Chem. 2004, **43**, 5442-5449.
10 S. Vallejos, V. Khatko, J. Calderer, I. Gracia, C. Cané, E. Llobet and X. Correig, Sensors Actuat. B-Chem., 2008, **132**, 209-215.
11 J. Zhou, L. Gong, S. Z. Deng, J. Chen, J. C. She, N. S. Xu, R. Yang and Z. L. Wang, Appl. Phys. Lett., 2005, **87**, 223108-2231010.
12 F. Liu, T. Guo, Z. Xu, H. Gan, L. Li, J. Chen, S. Deng, N. Xu, D. Golberg and Y. Bando, J. Mater. Chem. C, 2013, **1**, 3217-3225.
13 K. Yusuke, K. Keigo, O. Takeshi, N. Keisuke, T. Kentaro and N. Masayuki, Jpn. J. Appl. Phys., 2007, **46**, 6250-.
14 R. Schlaf, H. Murata and Z. H. Kafafi, J. Electron Spectrosc., 2001, **120**, 149-154.
15 C. X. Zhao, Y. Li, Y. Chen, J. Wu, B. Wang, F. Yi, S. Deng, N. Xu and J. Chen, Nanotechnology, 2013, **24**, 275703-275711.
16 J. M. Sun, N. Xu, Y. W. Cao, J. N. Yao and E. G. Wang, J. Mater. Res., 2000, **15**, 927-933.
17 J. Y. Luo, F. L. Zhao, L. Gong, H. J. Chen, J. Zhou, Z. L. Li, S. Z. Deng and N. S. Xu, Appl. Phys. Lett., 2007, **91**,093124-093106.
18 Y. Baek and K. Yong, J. Phys. Chem. C, 2007, **111**, 1213-1218.
19 A. Georg, W. Graf, R. Neumann and V. Wittwer, Solid State Ionics, 2000, **127**, 319-328.
20 T. Yoshimura, J. Appl. Phys., 1985, **57**, 911-919.
21 J. Y. Luo, W. Li, F. Chen, X. X. Chen, W. Da Li, H. Y. Wu, Y. J. Gao and Q. G. Zeng, Sensors Actuat B-Chem., 2014, **197**, 81-86.